Electrostatic Binding and Hydrophobic Collapse of Peptide–Nucleic Acid Aggregates Quantified Using Force Spectroscopy

Joan Camunas-Soler,[†,‡] Silvia Frutos,[†,‡] Cristiano V. Bizarro,[†,‡,⊗] Sara de Lorenzo,[†,‡] Maria Eugenia Fuentes-Perez,[§] Roland Ramsch,[‡,⊥] Susana Vilchez,[‡,⊥] Conxita Solans,[‡,⊥] Fernando Moreno-Herrero,[§] Fernando Albericio,[‡,∥,#,△] Ramón Eritja,[‡,⊥,∥] Ernest Giralt,[‡,∥] Sukhendu B. Dev,[∥] and Felix Ritort[†,‡,*]

[†]Small Biosystems Lab, Departament de Física Fonamental, Universitat de Barcelona, Avinguda Diagonal 647, 08028 Barcelona, Spain, [‡]CIBER de Bioingeniería, Biomateriales y Nanomedicina, Instituto de Salud Carlos III, Madrid, Spain, [§]Centro Nacional de Biotecnología, CSIC, 28049 Cantoblanco, Madrid, Spain, [⊥]Institut de Química Avançada de Catalunya, Consejo Superior de Investigaciones Científicas (IQAC—CSIC), 08034 Barcelona, Spain, [∥]Institute for Research in Biomedicine (IRB Barcelona), Barcelona Science Park, Baldiri Reixac 10-12, 08028 Barcelona, Spain, [#]Department of Organic Chemistry, University of Barcelona, 08028 Barcelona, Spain, and [△]School of Chemistry and Physics, University of KwaZulu-Natal, 4001-Durban, South Africa. [⊗]Present address: (C.V.B.) Centro de Pesquisas em Biologia Molecular e Funcional/PUCRS Avenida Ipiranga 6681, Tecnopuc, Partenon 90619-900, Porto Alegre, RS, Brazil.

ABSTRACT

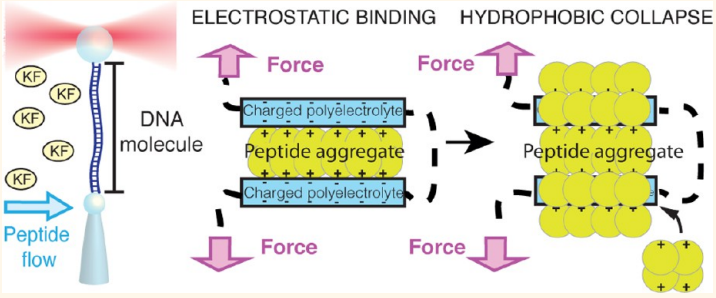

Knowledge of the mechanisms of interaction between self-aggregating peptides and nucleic acids or other polyanions is key to the understanding of many aggregation processes underlying several human diseases (*e.g.*, Alzheimer's and Parkinson's diseases). Determining the affinity and kinetic steps of such interactions is challenging due to the competition between hydrophobic self-aggregating forces and electrostatic binding forces. Kahalalide F (KF) is an anticancer hydrophobic peptide that contains a single positive charge that confers strong aggregative properties with polyanions. This makes KF an ideal model to elucidate the mechanisms by which self-aggregation competes with binding to a strongly charged polyelectrolyte such as DNA. We use optical tweezers to apply mechanical forces to single DNA molecules and show that KF and DNA interact in a two-step kinetic process promoted by the electrostatic binding of DNA to the aggregate surface followed by the stabilization of the complex due to hydrophobic interactions. From the measured pulling curves we determine the spectrum of binding affinities, kinetic barriers, and lengths of DNA segments sequestered within the KF—DNA complex. We find there is a capture distance beyond which the complex collapses into compact aggregates stabilized by strong hydrophobic forces and discuss how the bending rigidity of the nucleic acid affects this process. We hypothesize that within an *in vivo* context, the enhanced electrostatic interaction of KF due to its aggregation might mediate the binding to other polyanions. The proposed methodology should be useful to quantitatively characterize other compounds or proteins in which the formation of aggregates is relevant.

KEYWORDS: DNA condensation · aggregation · single molecule · force spectroscopy · DNA—peptide complex · optical tweezers

Understanding the driving forces by which self-aggregating molecules bind their targets inside the cell is of the utmost importance to elucidate their mechanisms of action.[1−7] Self-aggregating peptides bearing a definite charge are able to establish strong electrostatic interactions with oppositely charged polymers. In particular, recent bulk studies have shown that amyloid peptides with positive charges (*e.g.*, human lysozyme, Aβ40, α-synuclein, histidine-leucine peptides) have a strong binding affinity to negatively charged polymers (*e.g.*, nucleic acids, polysaccharides, polylysines), stimulating aggregation and fibril formation.[1,8−13] Such ubiquitous interaction has triggered

* Address correspondence to fritort@gmail.com.

Received for review February 12, 2013 and accepted May 24, 2013.

Published online May 24, 2013
10.1021/nn4007237

discussions on its connection to neurodegenerative diseases and on the hypothetical role of aggregating peptides as scaffolds for polynucleotide assembly in early prebiotic life.[1,14] Despite their prevalence, and even though much progress has happened within the past few years, the complex and nonspecific nature of these interactions makes it difficult to quantitatively determine key parameters such as their binding affinities and the kinetic steps during the interaction process.

Indeed, a full characterization of the interaction between hydrophobic peptides and polyanions is challenging due to the competition between peptide–peptide self-aggregating interactions and peptide–substrate electrostatic binding forces, as well as due to the transient and heterogeneous nature of the formed complexes.[11] An excellent model to address such questions is the anticancer drug kahalalide F (KF), a 14-residue cyclic depsipeptide originally isolated from the Hawaiian mollusk *Elysia rufescens*.[15] KF is a low-solubility compound with a highly hydrophobic structure and a single positive residue (L-ornithine) (Figure 1),[16] which exhibits a potent cytotoxic activity against several tumor cell lines,[17−19] causing the disruption of the plasma membrane due to the accumulation of peptide aggregates.[20] Although KF is a molecule with a strong tendency to aggregate, it also has a single positive charge capable of establishing electrostatic interactions with negatively charged substrates such as DNA. Here we use optical tweezers, AFM imaging, and dynamic light scattering (DLS) to fully characterize the interaction of KF aggregates binding to DNA. Although the formation of KF–DNA complexes can be directly observed in AFM and DLS measurements, only force spectroscopy methods make it possible to quantitatively determine the driving thermodynamic forces. In addition, by applying mechanical force to the ends of the DNA it is possible to control and gain insight into the kinetic steps involved in the formation of the complex.

We have found that binding of DNA to KF occurs in two kinetic steps: First, DNA binds KF particles due to the electrostatic attraction between the negatively charged DNA and the positively charged groups exposed on their surface (L-Orn). Electrostatic binding compacts DNA by sequestering DNA segments along the surface of the aggregate in a way reminiscent of a condensation process. This is followed by a slow remodeling of hydrophobic contacts and the irreversible entrapping of DNA within the KF–DNA complex. Modeling of the stretching curves yielded characteristic parameters of the interaction, such as the average length of DNA segments electrostatically bound to the aggregate, their affinity of binding, and the barrier to unpeel them. DNA unzipping experiments show that KF also forms complexes with ssDNA. However the different mechanical (bending rigidity) and chemical (hydrophobicity) properties of the polyelectrolyte determine the kinetics of formation of the complex.

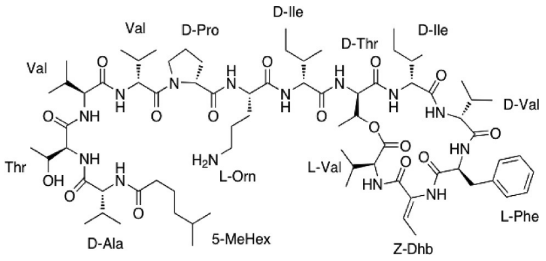

Figure 1. Kahalalide F structure.

RESULTS

KF Compacts dsDNA. To study how KF binds DNA, we stretched a single half λ-DNA (24-kb) in the presence of KF in the optical tweezers setup (Figure 2a, inset). First a DNA molecule was tethered between two beads, and its elastic properties were measured using the worm-like chain (WLC) model (see Materials and Methods). Next the DNA molecule was rinsed with 40 μM KF while it was maintained at an end-to-end distance of 6 μm. In this configuration the DNA can explore bended conformations due to thermal fluctuations, as the force remains below 0.4 pN at this extension. The flow was temporarily stopped after 5, 15, and 30 min in order to record a series of force–extension curves (Figure 2a). We collected measurements for at least 10 different molecules, finding a reproducible pattern (Figure S1, Supporting Information).

After flowing KF for 5 min, DNA maintained at low tension was compacted by the peptide. In order to stretch the compacted molecule, the KF–DNA complex must be unraveled, and therefore a sawtooth pattern with many force rips was observed (Figure 2a, purple). This suggests that KF behaves as a DNA condensing agent, inducing kinks and loops on the DNA. The relaxation curves, however, remained similar to those obtained for naked DNA (Figure 2a, black), indicating that DNA compaction took place after the extension of the molecule was reduced. The relaxation curves were well described by the WLC model and showed a decrease of 25% in the persistence length (Figure 2b, inset). In experiments where KF was flowed for 5 or 15 min, the whole contour length of the DNA could be recovered after pulling up to 40 pN (Figure 2c). This reduction of the persistence length is likely due to the positively charged L-Orn residue, which decreases the self-repulsion of the DNA phosphate backbone.

However, after 15 to 30 min, many interactions could not be disrupted, leading to an apparent shorter contour length, which was correlated to an increase of the persistence length. This phenomenon suggests that the KF–DNA complex started to collapse into a more stable and stiffer structure after 15 min. Remarkably, a repulsive negative force was detected after 30 min in

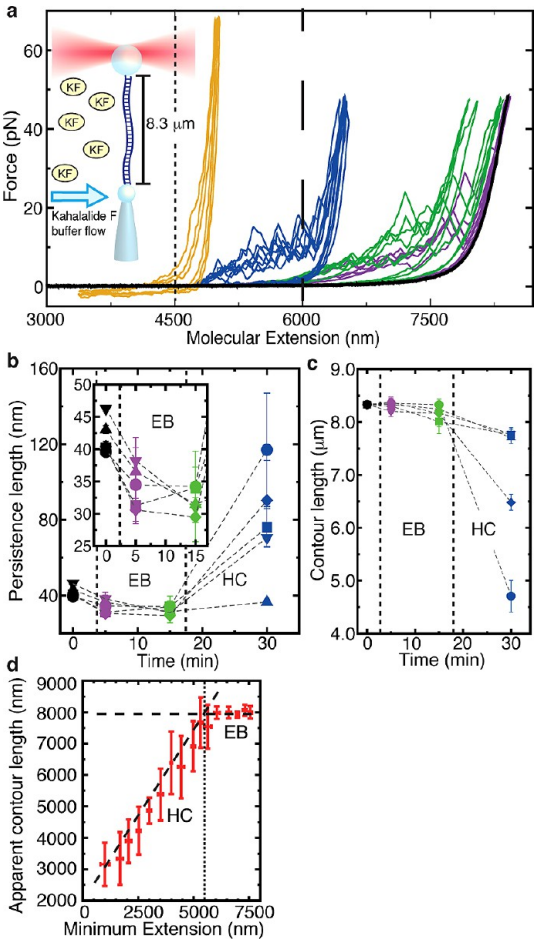

Figure 2. KF binds to dsDNA. (a) DNA pulling curves before (black) and after flowing KF at different waiting times: 5 min (purple), 15 min (green), and 30 min (blue). The molecule is maintained at an extension of 6 μm (vertical dashed line), and the flow is temporarily stopped to perform pulling cycles between a minimum extension of 4.5 μm (dotted line) and a maximum force of 45 pN. The sawtooth pattern observed indicates that KF induces the compaction of DNA. Pulling cycles reaching end-to-end distances lower than 4 μm are shown in yellow. Data are filtered at 10 Hz bandwidth, v = 500 nm/s. (Inset) Experimental setup. (b, c) Persistence and contour length of five DNA molecules after flowing KF (black corresponds to naked DNA). The changes in the elastic parameters are a signature of the two regimes observed in KF–DNA complex formation: electrostatic binding and hydrophobic collapse. (d) Apparent contour length of a DNA molecule repeatedly pulled between a maximum force of 40 pN and a minimum extension that decreases in steps of 500 nm per pulling cycle (mean ± SD, N = 10).

most of the experiments if end-to-end distances lower than 4 μm were allowed (Figure 2a, yellow), suggesting the formation of a thick KF–DNA aggregate of 1–3 μm in length. It was not possible to remove the bound KF by rinsing the molecule with peptide-free buffer for more than 45 min, reflecting the high stability of the final complex.

Binding of KF to DNA exhibits two regimes. First, there is a weak and fast regime apparently determined by the electrostatic attraction between the positively charged residues of the KF particles and the negatively charged backbone of DNA. According to our interpretation, in this regime DNA binds to hydrophilic spots exposed on the surface of KF particles. Unpeeling of DNA segments requires forces typically lower than 20 pN. We will refer to this mode of binding as electrostatic binding (EB). This regime is observed in the first 15 min of the experiments shown in Figure 2a and is characterized by a constant contour length, the presence of force rips associated with unpeeling events, and a reduced persistence length; the increased flexibility of the filament indicates a charge compensation that reduces self-repulsion of phosphates along the DNA backbone. There is a second stronger binding regime that occurs over longer time scales, which we attribute to the formation of an increasing number of stable hydrophobic contacts within the growing KF–DNA complex. Our interpretation is that in this regime DNA gets buried inside the bulk of the aggregate after being recruited by the hydrophilic spots exposed on its surface, creating a stiff filament (as suggested by its increased persistence length). The slower time scales observed in this regime suggest that this mode of binding requires the remodeling and growth of a strongly hydrophobic complex. We will therefore refer to this second regime as hydrophobic collapse (HC). It is characterized by an irreversible decrease in contour length, an increase in persistence length, and the final collapse of the KF–DNA complex that is eventually compressed by pushing the two beads closer than 4 μm. The force required to disrupt this HC structure is above those accessible with our setup (~100 pN), as suggested from previous AFM pulling experiments of single hydrophobically collapsed polymers.[21]

What is the parameter that controls the prevalence of each binding regime? We expect that DNA bending fluctuations determine its binding to KF and the subsequent stabilization of the complex. Therefore, the molecular extension—or distance between beads—should be the parameter controlling the transition between both regimes. To verify this hypothesis, we carried out experiments where the DNA was repeatedly pulled in the presence of KF between a maximum force of 40 pN and a minimum extension that progressively decreased from 8 to 2 μm in steps of 500 nm per pulling cycle. Such minimum extension controls the degree of compaction reached by the complex. For each cycle we then measured the apparent contour length at the maximum force (40 pN). The results (Figure 2d) confirm the presence of the aforementioned regimes, which are separated by a threshold capture distance of 5.5 μm (corresponding to 66% of the contour length of the molecule). In the EB regime (relative extension ≥66%) the apparent contour length of the DNA fiber does not change, whereas in the HC regime (relative extension ≤66%) it decreases linearly with the minimum distance between the two beads. A KF analogue in which the ornithine residue was

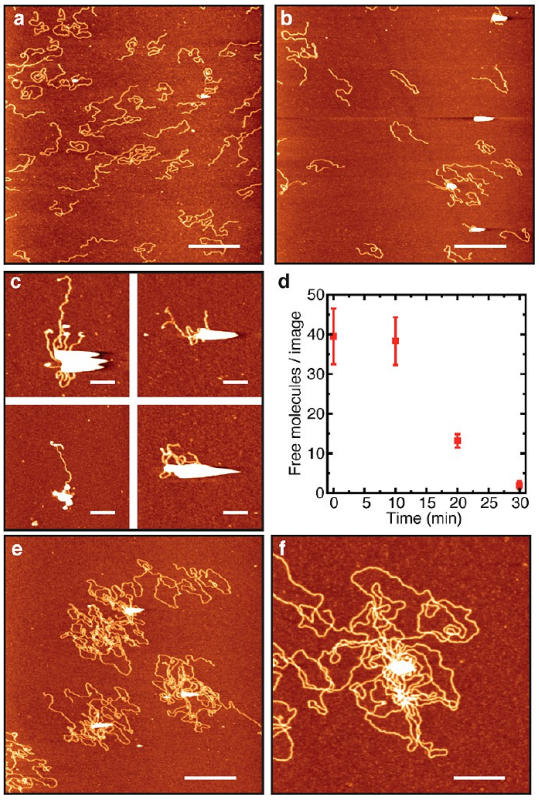

Figure 3. AFM images of KF−DNA complexes. (a−c) AFM images of reactions of 1.65 ng linearized pGEM plasmid (2743-bp) and 100 μM KF obtained at 0, 20, and 30 min incubation times at room temperature, respectively. The number of free DNA molecules decreases with incubation time, and large compaction blobs are observed. (d) DNA surface density at different incubation times, determined as the average number of free individual molecules per image of 9 μm^2 (mean $\pm$ SD, $N \geq 6$). (e, f) Full λ-DNA (48-kb) incubated with 100 μM KF for 30 min. DNA condensation and formation of blobs are also seen for this larger DNA substrate. Bar scale is 600 nm (a, b, e) and 200 nm (c, f). Color scale (from dark to bright) is 0−2 nm in all AFM images.

replaced by a negatively charged glutamic acid was investigated. No interaction between the KF analogue and DNA was observed (Figure S2, Supporting Information), confirming that the positive charge of the ornithine residue is essential for electrostatic binding and providing further evidence that electrostatic interactions are key for the initial binding of the peptide to DNA. As well, a salt titration showed that the initial binding of KF to DNA and the subsequent DNA compaction is highly dependent on the ionic strength of the buffer, in agreement with the proposed mechanism (Figure S3, Supporting Information).

The formation of KF−DNA aggregates was directly observed by AFM imaging using a 2743-bp DNA fragment (Figure 3a−c). Formation of blobs was observed at the initial time of mixing, and their average size and number increased with time. Notably, after 20 min, a sharp decrease in the number of individual molecules bound to the mica surface was observed (Figure 3d). We attribute this to the formation of intermolecular complexes in which several DNA molecules are recruited into a single aggregate. As a consequence, no free DNA was observed after 30 min incubation time. These results were further confirmed with the use of longer DNA molecules (λ-DNA, 48-kb, Figure 3e,f). In the absence of DNA, large aggregates were not found on the images (Figure S4, Supporting Information). The observed aggregation of KF and binding to DNA were also characterized with DLS (Section S2, Supporting Information). The hydrodynamic radius of KF aggregates increased with time and remained constant after addition of DNA.

KF−DNA Affinity Measurements in the EB Regime. Pulling experiments of DNA in the presence of KF show a force−distance curve pattern with force rips and hysteresis even if the pulling is performed at very low speeds (Figure 4a, blue). Low pulling speeds are particularly useful to characterize the affinity of DNA binding to KF aggregates during the EB regime. In these experiments, the slope between two consecutive force rips reflects the elastic response of DNA with a given apparent contour length l_0. Each force rip is due to the unpeeling of a DNA segment that was electrostatically bound to the KF particle. A statistical analysis of force rips was used to determine the length of the DNA segments released during the unpeeling process (see Materials and Methods).[22] In this way, each experimental data point was associated to an apparent contour length l_0 (Figure 4a, red left). A histogram of all the l_0 values showed a series of peaks that identify states that are stabilized by KF−DNA contacts (Figure 4a, red right). The distance between two consecutive peaks is the length of the DNA segment released at every unpeeling event. The histogram was then fitted to a sum of Gaussians (Figure 4a, bottom), and the distance between the mean of consecutive peaks was calculated. The experimental distribution of unpeeling events is broad (from a few nm to ~400 nm) and follows an exponential distribution with mean size $\Delta l_0^* = 31 \pm 6$ nm (Figure 4b). An exponential distribution of unpeeling lengths is known to correspond to the distribution of intervals expected in random partitioning a given contour length, in agreement with our hypothesis that DNA binds KF aggregates at hydrophilic spots in a random fashion.

A force *vs* contour length representation (Figure 4c) emphasizes the release of DNA segments in a stepwise manner during the unpeeling process. The mechanical work performed at each unpeeling event ($W = F\Delta x$) was then inferred from the rupture force value and released extension (see Materials and Methods). A histogram of the dissipated work (Figure S5, Supporting Information) shows an exponential distribution with average unpeeling energy of 13.5 $\pm$ 5 kcal/mol. This value sets an upper limit to the free energy of binding of KF to DNA.

To gain a better understanding of the affinity of DNA binding to KF particles, we used a simple

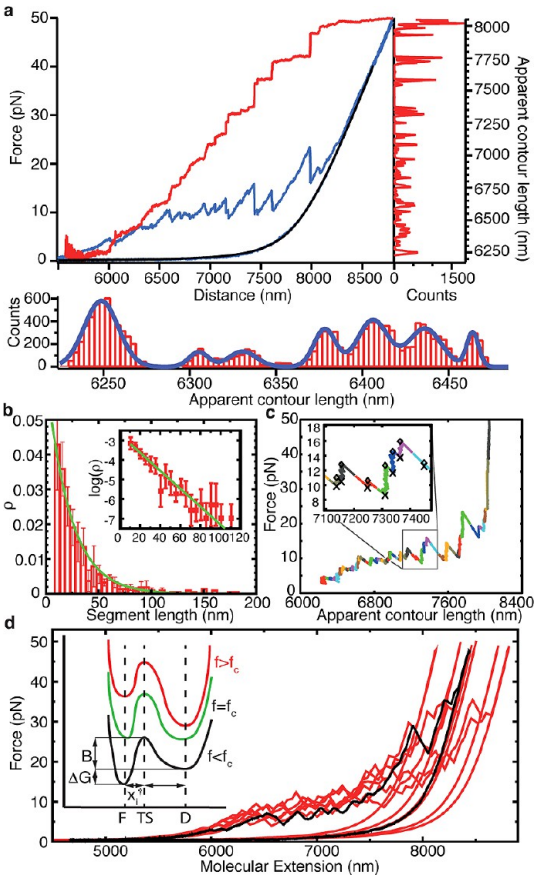

Figure 4. Modeling of DNA stretching experiments. (a) (Top, left) Blue curve shows a typical force−distance curve in a KF−DNA pulling experiment (20 Hz bandwidth, v = 30 nm/s). Red curve shows the apparent contour length l_0 (right axis) for each experimental data point. The release cycle is fitted to the WLC model (black). (Top, right) Histogram of l_0 values. (Bottom) Detailed view of the histogram (red) and fit to a sum of Gaussians (blue). (b) Histogram of unpeeling segment lengths Δl_0 and fit to an exponential distribution (green). Inset shows a log-normal plot (mean ± SD, N = 435 events, 3 molecules). (c) Force *vs* apparent contour length representation of the pulling experiment. Each color identifies a state (apparent contour length) temporally stabilized by KF−DNA contacts during the unpeeling process. (Inset) Sharp transitions between states are observed. Minimum and maximum forces of every state are indicated with crosses and diamonds, respectively. (d) The black curve is an experimental pulling curve after 15 min interaction with KF (v = 500 nm/s). A set of six simulations of the theoretical model is shown in red. (Inset) Scheme of the free-energy landscape of a two-state system at different forces (f). The main parameters describing the system are the free energy difference (ΔG) between the formed (F) and dissociated (D) conformations, the height of the barrier (B), the distance (x_i) separating the two conformations, and the distance ($x_i^\dagger$) from the transition state (TS) to the formed conformation. As the force is increased, the free-energy landscape is tilted favoring the dissociated conformation once the critical force (f_c) is reached.

theoretical model that reproduces the experimental force−extension curves. We considered a model previously used to characterize the DNA−dendrimer condensation transition (see Materials and Methods).[23] The model reproduces the essential features of the experimental curves (Figure 4d) over a wide range of pulling speeds (30−500 nm/s). Despite the apparent large number of free parameters, only certain values in very specific ranges can reproduce these features (Section S3, Supporting Information). In brief, the experimental force−extension curves could be well described by assuming (a) a low binding energy of DNA to KF aggregates ($\Delta G \approx 6 \pm 2$ kcal/mol); (b) a brittle unpeeling of the DNA segments ($x_i^\dagger = 2 \pm 1$ nm, the barrier lying close to the formed conformation); and (c) a broad right-tailed distribution $p(B)$ of high-energy activation barriers given by $p(B) = (1/w') \exp[-(B - B_0)/w']$ with $B \geq B_0 = 89\ k_BT$ and $w' = 5\ k_BT$.

DNA Binds to KF Aggregates at Forces Lower than 1 pN. We followed the kinetics of DNA compaction by performing constant-force experiments at forces such that EB prevails (molecular extension ≥5.5 μm, Figure 2d). The DNA molecule was maintained at constant force using force feedback, and we followed the time evolution of the molecular extension while KF was flowed in.

At 1 pN, a fast compaction took place (Figure 5a). The extension was reduced up to 40% in 20 min at a reproducible rate. This compaction is characterized by intermittent drops of extension that shorten the molecule by hundreds of nanometers in a few seconds (Figure 5a, arrows). Pulling curves performed after this experiment (Figure 5b) showed again the characteristic sawtooth pattern.

In contrast, at 5 pN the molecular extension remained constant within 100 nm after flowing KF for more than 30 min (Figure 5c). Still, intermittent large fluctuations on the order of tens of nanometers were often detected (Figure 5c, arrows). These large fluctuations were never observed in controls without KF (Figure 5c, gray), and we attribute them to individual binding events. Pulling cycles performed between 5 and 40 pN immediately after the peptide flow show a slight decrease in the persistence length and weak hysteresis effects, suggesting very weak binding of DNA to KF (Figure 5d). Only by further decreasing the extension and force of the molecule were full binding events observed (Figure 5d).

Interestingly an overstretching transition was not always observed (Figure 5d, yellow). We attribute this to the recruitment of DNA segments close to both ends of the tethered molecule by KF particles that induce a torsionally constrained fiber, inhibiting the overstretching transition (Figure 5d, inset).[24] Otherwise, KF binding does not suppress or tilt the overstretching plateau as observed for DNA intercalators.[25] Moreover, the characteristic sawtooth pattern of KF remained visible after fully overstretching the DNA (Figure S6, Supporting Information).

Unzipping Experiments Reveal Different Binding Modes of KF to dsDNA and ssDNA. In a different setup (Figure 6a), a 6.8-kb DNA hairpin was tethered and partially unzipped, maintaining at least half of the dsDNA stem open (Figure 6a, dashed line), and then KF was flowed into

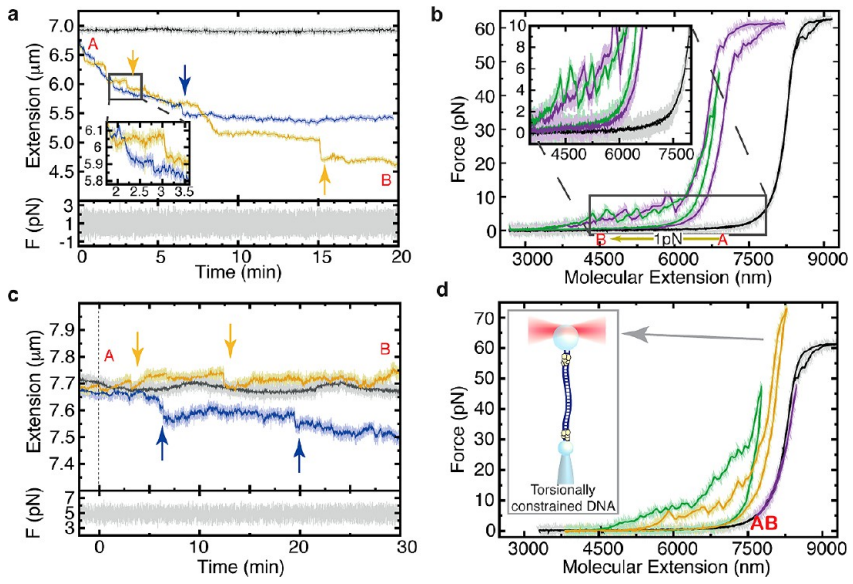

Figure 5. Kinetics of DNA binding to KF particles at a constant force. (a) DNA compaction at 1 pN. A control without peptide (gray) and two equivalent experiments at 40 μM KF (blue and yellow) are shown. The molecule was maintained at an initial extension A that relaxed at constant force down to a final value B. (b) Stretching of a DNA molecule before (black) and after (green, purple) the constant-force experiment at 1 pN. (c) KF does not compact DNA at 5 pN. A DNA molecule subjected at 5 pN is rinsed with KF, and changes in the molecular extension are monitored. A control experiment without peptide (gray) and two independent experiments at 40 μM KF (blue and yellow) are shown. Large fluctuations indicative of individual binding events are observed (arrows). (d) Stretching of a DNA molecule only at forces higher than 5 pN immediately after the constant-force experiment at 5 pN (purple). If the force was relaxed below 5 pN (green and yellow), the characteristic sawtooth pattern was immediately recovered. The force–extension curve of that molecule before flowing KF is shown in black. For all plots, raw data (1 kHz) are shown in light colors, and filtered data (1 Hz bandwidth for kinetic experiments, 10 Hz bandwidth for pulling experiments) are presented in dark colors. Pulling speed is 500 nm/s.

the chamber. In this configuration the released ssDNA is long but rigid enough to severely restrict thermal fluctuations in the molecular extension (rmsd ~20 nm). The advantage of this setup is that the long separation between the hairpin and the beads (~4 μm) inhibits any interaction between the beads and both the dsDNA region and linkers. The unzipping pattern of a DNA molecule is a fingerprint of its base sequence[26] (Figure 6a, gray), and changes of that pattern indicate a direct interaction between the peptide and DNA. Moreover, with this setup we could explore the effect of KF on a DNA molecule maintained at zero force and forming a random coil (the force stretches the linkers but not the hairpin).

After flowing KF for 3 min, the unzipping pattern substantially changed (Figure 6a), and forces up to 22 pN were needed to unzip the DNA. We attribute this to the increased force required to simultaneously break the base-pairing interactions and unpeel DNA segments from the KF particles. Consecutive unzipping curves show that ssDNA remains bound to KF particles at the maximum forces (25 pN). Surprisingly enough, the rezipping trajectories overlapped with the rezipping curves of naked DNA over a wide range of extensions (≥1500 nm). This is in agreement with a reannealing mechanism in which rehybridization takes place first, followed by the formation of the complex. A similar phenomenon has been observed in the formation of amyloid nucleic acid fibers, in which the binding of amyloid peptides to oligonucleotides promotes their hybridization.[8]

Note that in this experiment we unzipped only the region of the hairpin that remained in double-stranded form while KF is flowed (right of the dashed line in Figure 6b). However, when we tried to rezip the region of the hairpin that remained as ssDNA during the peptide flow (left of the dashed line in Figure 6b), we could not recover the characteristic unzipping pattern of the molecule. This indicates that KF can bind ssDNA in a way that prevents rehybridization of ssDNA strands. If the molecule was continuously submitted to unzipping/rezipping cycles, the region of the DNA hairpin that previously rezipped progressively loses that capability (Figure 6c), suggesting that KF is slowly binding to the stretched ssDNA (arrow in Figure 6c).

These results suggest that KF binds to the phosphate backbone in a configuration that does not interfere with base-pairing interactions when DNA is in its double-stranded form. However, when DNA is in its single-stranded form, KF can adopt configurations that interfere with the rezipping of the molecule. These experiments also show that the interaction of the peptide with ssDNA is slow (on the order of minutes), as only the ssDNA regions of the hairpin that remained exposed for long times to the peptide were unable to rehybridize.

KF Binds ssDNA. To characterize the interaction of ssDNA with KF aggregates, we developed a simple

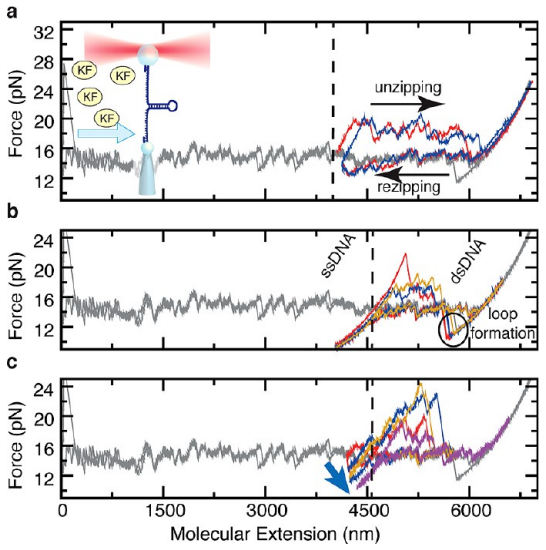

Figure 6. Unzipping experiments show that KF binds both dsDNA and ssDNA. (a) An unzipping pattern of the DNA hairpin before incubation with KF is fully represented in gray in each panel. The dashed line represents the position at which the molecule remained unzipped during the peptide flow. Consecutive pulling cycles of the dsDNA stem region after incubation with KF (blue, red) show a strong distortion of the unzipping pattern. However, the rezipping of the hairpin remains unaffected, indicating that the molecule can hybridize again. (Inset) A 6.8-kb hairpin is maintained partially unzipped, leaving less than half of the dsDNA stem closed during the incubation with KF. This configuration prevents KF−DNA interactions mediated by the beads. (b) The region of the hairpin that remained as ssDNA during the peptide flow (left of dashed line) cannot hybridize again, in contrast to what happens without KF (gray curve) or in the region maintained as dsDNA during the peptide flow (right of dashed line). Three pulling cycles are plotted in blue, red, and yellow. (c) If the hairpin is rinsed with KF and then submitted to several consecutive pulling cycles, the nonhybridizing region increases with time. Four pulling cycles that reflect this trend are shown (red, blue, yellow, and purple). Data are filtered at 10 Hz bandwidth, v = 50 nm/s.

method to generate a long ssDNA template (13-kb) for optical tweezers experiments (see Materials and Methods). By using this setup we could therefore measure the elastic response of the ssDNA down to forces as low as 1−2 pN (Figure 7a).

We then followed their molecular extension in the presence of KF. At 5 pN we observed a slow compaction (∼20−30 min) with an absolute reduction in extension close to 16% (Figure 7b, upper panel), demonstrating that ssDNA binds KF. This compaction was reproducible within different experiments, and the slow kinetics agree with the results from unzipping experiments (Figure 6c). We also measured the time evolution of the stiffness of the KF-ssDNA fiber by recording the magnitude of the thermally induced fluctuations in the molecular extension (Section S4, Supporting Information). At 5 pN the molecule stiffened with time at a rate of $(13 \pm 5) \times 10^{-3}$ pN/(nm·s) (Figure 7b, middle panel). However this change was observed only 10−15 min after compaction of the fiber started, suggesting that stiffness changes are mostly due to the hydrophobic collapse of the KF-ssDNA aggregate rather than electrostatic binding of ssDNA to KF particles.

Pulling curves obtained after the peptide flow (Figure 7c) also show force rips in the stretching curves. However the sawtooth pattern was smoother than for dsDNA, suggesting the occurrence of fewer events and higher unpeeling forces (Figure 7c). We attribute this to the increased hydrophobic forces that stabilize the KF−ssDNA complex, which also lead to a systematic shortening of the effective contour length of the ssDNA. At a higher stretching force of 10 pN, KF did not induce compaction of ssDNA though, but intermittent jumps in the extension were observed, indicative of individual binding events (Figure S7a, Supporting Information). At this higher force, the stiffness of the molecule remained constant within the resolution of measurements (Figure S7b, Supporting Information). However, KF−ssDNA compaction could be induced by lowering the force to 5 pN (Figure S7a, Supporting Information), reproducing the results reported in Figure 7b.

Binding of ssDNA to KF aggregates was further corroborated by AFM. ssDNA molecules (2743-bp) were generated by heat denaturation and fast cooling to 4 °C (Figure 7d). Addition of KF to the ssDNA preparation triggered the formation of aggregation spots immediately after mixing (Figure 7e). Interestingly enough, longer incubation times yielded a reduction of free ssDNA molecules, together with the formation of large aggregates of KF surrounded by double-stranded DNA (Figure 7f,g). This observation suggests that KF induces the rehybridization of ssDNA, as ssDNA molecules do not anneal after 30 min incubation at room temperature in the absence of KF. This is in agreement with the unzipping results (see previous section) and is likely due to the fact that KF traps and maintains close in space different ssDNA molecules that are occasionally able to rehybridize.

DISCUSSION

By combining single-molecule techniques and bulk measurements we showed that KF forms particles that bind and compact DNA. Our measurements reveal that this process is characterized by two distinct phases controlled by the molecular extension of the DNA. First, there is a fast and weak binding regime determined by electrostatic binding to positive residues exposed on the surface of the KF particles (Figure 8a). This binding is triggered by spontaneous bending fluctuations along DNA. Upon reduction of the molecular extension, a slow remodeling of the KF−DNA complex takes place; we propose that this new regime is led by the formation of new hydrophobic contacts that stabilize a hydrophobically collapsed structure. A capture distance separating both regimes is identified, corresponding

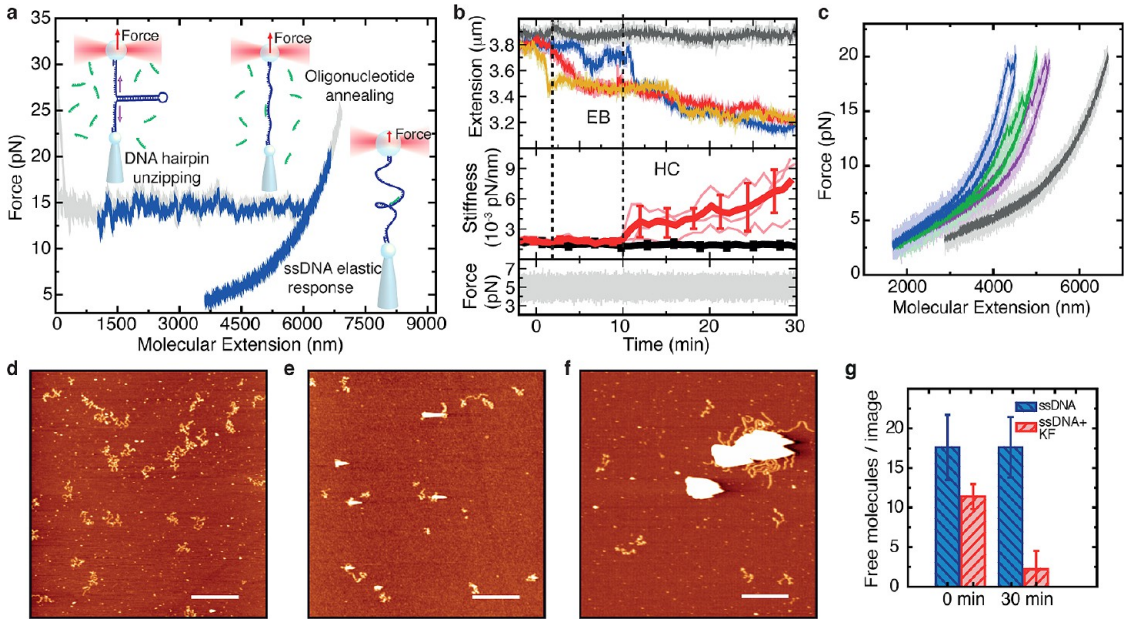

Figure 7. Kinetics of ssDNA binding to KF particles. (a) Method used to generate a long ssDNA template from a DNA hairpin. The specific binding of an oligonucleotide to the hairpin inhibits the hybridization of the molecule (blue) at forces lower than the average unzipping force. The full force−extension curve of the hairpin is plotted as a reference (gray). (b) Compaction and stiffening of ssDNA at 5 pN are representative of EB and HC, respectively. (Top) Extension of a ssDNA molecule rinsed with KF at 5 pN. Three independent experiments at 40 μM KF (blue, red, and yellow) and a control without peptide (gray) are shown (compaction starts at t = 0). (Middle) Average stiffness of the ssDNA molecule at 5 pN during the peptide flow (red) and a control without peptide (black). Three individual experiments are shown in light red. The stiffness is measured from the fluctuations in the trap position. (c) Stretching curves of a ssDNA molecule before (gray) and after incubation with 40 μM KF at 3 pN for 25 min (purple, green, and blue). Data are collected at 1 kHz (light colors) and filtered to 1 Hz bandwidth (dark colors). Pulling speed is 100 nm/s. (d) ssDNA molecules (1.8 nM molecules, 5 μM nucleotides) are adsorbed on a mica surface showing a more compact conformation than dsDNA due to its lower persistence length. (e) Immediately after mixing KF (100 μM) with ssDNA molecules (5 μM nucleotides) we observe the formation of aggregation spots and a substantial decrease in the number of ssDNA molecules per image. (f) After 30 min incubation at room temperature, these effects are more evident as big aggregates are seen. (g) Histogram of ssDNA molecules at different incubation times (0 and 30 min) with and without KF, determined as the average number of free individual molecules per image of 4 μm^2 (mean ± SD, $N \geq 6$).

to a relative extension of 66%. Remarkably enough, theoretical studies between spherical charged aggregates and oppositely charged polymeric chains predicted a capture distance leading to the irreversible adsorption of the chain to the aggregates.[27] The recruitment of DNA segments along the surface of the aggregate (EB) is driven by the electrostatic attraction between the negative charge of DNA and the positive charge of L-Orn residues that are most likely exposed on the surface of the particle forming hydrophilic spots (Figure 8b). This interpretation is supported by the following facts: (i) The persistence length of DNA is reduced during the initial binding of the peptide, suggesting a charge compensation that reduces self-repulsion of the DNA phosphate backbone (ii) A KF analogue without a positive charge does not bind to DNA (Figure S2, Supporting Information), providing evidence that the positive charge is essential for binding. (iii) A salt titration shows that binding of KF to DNA is inhibited at high salt condition and that the strength of the interaction increases with decreasing ionic strength (Figure S3, Supporting Information). (iv) The zeta-potential values of KF, DNA, and KF−DNA complexes (Table S1, Supporting Information) indicate different surface charge densities depending on whether DNA is complexed with KF or not.

In addition, the interaction observed during the EB regime cannot be understood from the isolated action of KF peptides (each bearing a single positive charge). It must be due instead to the concurrent action of several positive charges that are contained in each peptide aggregate, which are then able to electrostatically interact with DNA in a similar fashion that dendrimers or other polycationic agents do. Modeling of the experimental results shows that EB of DNA to KF particles is consistent with an exponential distribution of unpeeling lengths (average value $\Delta l_0 = 31 \pm 6$ nm), a low binding energy ($\Delta G \approx 6 \pm 2$ kcal/mol), a brittle unpeeling process ($x_i^{\dagger} = 2 \pm 1$ nm), and a disordered collection of activation barriers higher than $B_0 = 89 k_B T$ with an exponential right tail of width $w' = 5 k_B T$. This is in contrast to results obtained for nucleosomal particles that show a single characteristic unpeeling length of 26 nm and a single energy barrier of $(36-38) k_B T$.[28] The force at which we observe dsDNA compaction (1 pN) is in the same range of forces that has been reported for other DNA compacting molecules such as histone-like FIS and HU proteins[29,30] or polycationic condensing agents.[23,31,32]

Unzipping experiments show that KF also forms complexes with ssDNA. Interestingly, unzipping experiments

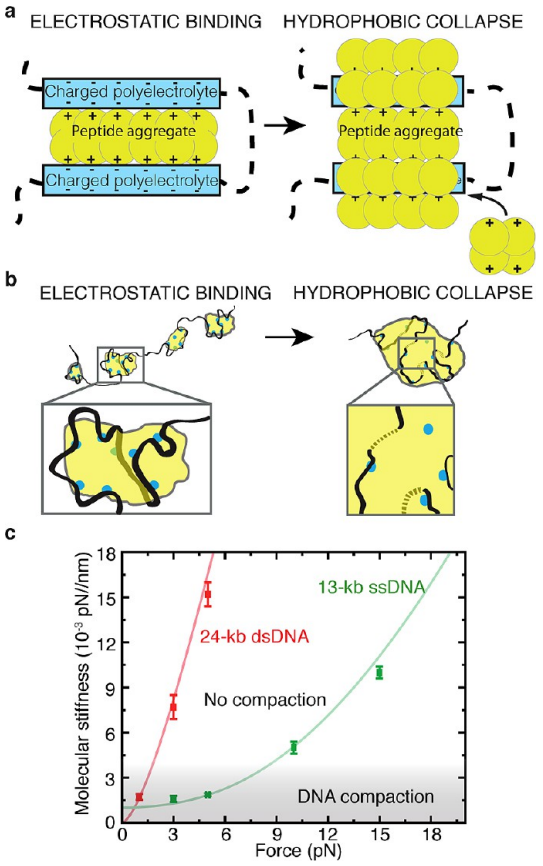

Figure 8. Model of KF−DNA complex formation. (a) Scheme of the two kinetic steps during the formation of the KF−DNA complex: electrostatic binding (EB) and hydrophobic collapse (HC). At low forces DNA (blue) binds to KF particles (yellow) due to the electrostatic attraction of the phosphate backbone to positive residues exposed on the aggregate surface (EB). This process is followed by the formation of new hydrophobic contacts between aggregates that form a larger collapsed structure (HC). (b) Pictorial representation of how bending fluctuations induce the EB of DNA (black) to electrophilic spots (blue) on the aggregate surface and how hydrophobic interactions between peptides lead to a collapsed structure in which DNA becomes entrapped within the aggregated complex. (c) Phase diagram showing conditions that trigger DNA compaction due to EB of KF in constant-force experiments. Average stiffness of the dsDNA (red) and ssDNA (green) molecules before flowing KF in the constant-force experiments ($2 \leq N \leq 9$, mean ± SD). We observe DNA compaction only in the region highlighted in gray, suggesting that compaction depends directly on DNA bending fluctuations *via* template stiffness. A WLC model (red line) and FJC model (green line) with the parameters determined in the main text for dsDNA and ssDNA, respectively, are plotted as a reference.

together with AFM show that KF does not inhibit dsDNA hybridization. These results agree with previous studies on the formation of amyloid nucleic acid fibers, which showed how charged surfaces of peptide complexes recruit oligonucleotides and promote their hybridization.[8] The two distinct phases observed in the formation of KF−dsDNA complexes (EB and HC) were also seen for ssDNA, showing that the mechanism of complexation is similar in both polyelectrolytes. Yet, our experiments suggest a stronger stabilization of the complex for ssDNA, which is likely due to its increased hydrophobicity and lower persistence length. Indeed, we have found that KF can compact ssDNA at higher forces than dsDNA does, indicating the role of spontaneous bending fluctuations to initiate EB. Finally, constant-force experiments with both DNA substrates show a correlation between the degree of compaction of the molecule and the effective rigidity of the tether (Figure 8c).

In relation to its biological activity, and as previously shown for amyloid fibrils,[1,9,13] the enhanced positive charge of KF aggregates could allow them to interact more effectively with other polyanionic molecules such as polysaccharides (*e.g.*, glycosaminoglycans). Whether or not the cytotoxic effects of KF are related to its interaction with polyanions, we hypothesize that these interactions could play a role in modulating the activity of the peptide either intracellularly or in the extracellular matrix. In particular KF might also interact with the phospholipids of the plasma membrane inducing the formation of pores and cell necrosis.[20]

CONCLUSION

This study represents the first attempt to extract quantitative information about the binding affinity and kinetic steps involved in the interaction between a nucleic acid (DNA) and an anticancer self-aggregating peptide (KF) at the single-molecule level. To date, most studies of aggregation kinetics have been performed using ensemble techniques where the individual behavior of molecules cannot be distinguished. Using optical tweezers, we have shown that KF binds DNA in two kinetic steps (an initial electrostatic binding that is followed by a hydrophobic collapse of the peptide−DNA complex) and characterized the spectrum of binding affinities, kinetics barriers, and lengths of DNA segments sequestered within the KF−DNA complex. The proposed methodology is not limited to the characterization of amorphous aggregates.[33] Protein aggregation, a topic of major interest due to the role of the aggregation of misfolded proteins in neurodegenerative diseases,[34] might be well addressed using single-molecule force spectroscopy. As well, AFM images of the nucleoid-associated proteins Dps[35,36] and of the drug cisplatin[37] are very similar to those we found here for KF−DNA, suggesting that many biochemical studies of protein complexes that face similar aggregation or compaction phenomena are susceptible of being studied with this approach. For instance, the aggregation of the splicing factor MBNL1 by mutant mRNA hairpins is at the core of myotonic dystrophy type I.[38,39] Research on the formation of these RNA−protein aggregates and of peptides that disrupt this interaction[40] could greatly benefit from the aforementioned approaches. Our study confirms force spectroscopy studies of single aggregates as potentially very useful to characterize the thermodynamic

and mechanical properties of nucleic acid–peptide complexes. On a longer term, the study of the mechanical response of aggregates related to many relevant neurodegenerative diseases could also be approached by using a peptide template instead of a DNA molecule.

MATERIALS AND METHODS

Optical Tweezers Setup. A miniaturized dual-beam optical tweezers instrument described in ref 26 has been used for the single-molecule experiments. A single optical trap is created by focusing two counter-propagating laser beams (λ = 845 nm, P = 200 mW) into the center of a fluidics chamber mounted on a motorized stage. The optical trap can be displaced in a range of 12 μm by using a pair of piezoelectric actuators mechanically coupled to the laser optical fibers. For manipulation with the optical tweezers, DNA molecules are differentially end-labeled with digoxigenins and biotins so each end of the molecule can specifically bind to antidigoxigenin and streptavidin-coated beads, respectively (Supporting Information). A single DNA molecule is then tethered between two polystyrene beads. One is placed on the tip of a micropipette, whereas the other one is confined in the optical trap (Figure 2a, inset). The molecule can be stretched by moving the trap relatively to the micropipette, and both the extension and force applied to it are determined in real time.

Force applied to the optically trapped bead is directly determined from the change in light momentum by measuring the deflection of the laser beams with position-sensing detectors (PSDs).[41] To measure the position of the optical trap, about 8% of the lasers light is split before entering the objective lenses and redirected to PSDs. In this way, trap displacements can be followed with sub-nanometer resolution. The relative molecular extension is inferred by subtracting the trap compliance (F/k) to the absolute displacement of the optical trap (trap stiffness = 70 pN/μm). The extension and force applied to the molecule can be recorded at 1 kHz rate, and a resolution of 0.1 pN is achieved.

Stretching Experiments of dsDNA and ssDNA. The persistence length (l_p) and stretch modulus (S) of each dsDNA molecule were determined before flowing KF with a fit to the WLC model. Average values of l_p = 44.7 ± 2.0 nm and S = 1419 ± 240 pN were obtained (N = 10), in good accordance with the generally accepted parameters.[42−44] A compatible value of l_p = 43.0 ± 2.0 nm was also found using the inextensible WLC model. The stretching curves also showed the characteristic overstretching plateau at a force of 62.5 ± 0.5 pN with an extension ~70% of the contour length. Molecules that showed an abnormally high hysteresis on the overstretching transition (generally attributed to highly nicked DNA molecules) were discarded. For the fits to the WLC model, the correction to the Marko–Siggia interpolation formula suggested in ref 45 was used, and a Levenberg–Marquadt algorithm was used for both minimizations.[46] Details of the experimental setup and molecular synthesis are found in the Supporting Information.

To generate a 13-kb ssDNA molecule, a 6.8-kb DNA hairpin was fully unzipped in a buffer containing a 30-base oligonucleotide that binds to the loop and its flanking region due to base-pair complementarity. The high bending rigidity of the duplex at the loop region strongly stabilizes the ssDNA form over the dsDNA form at forces lower than the average unzipping force (14.5 pN). Stretching curves of the ssDNA molecule were fitted to the freely jointed chain model (Section S5, Supporting Information), finding a Kuhn length of b = 1.57 ± 0.05 nm (N = 5) in agreement with previous results.[26,42]

Statistical Analysis and Simulations. For every data point (x_{exp}, f_{exp}) of a force–distance curve, we determined its most probable apparent contour length (l_0) by finding the theoretical WLC[45] that passes closest to that point at the force f_{exp}:

$$|x_{exp} - x_{WLC}(l_0, f_{exp})| = \min_l (|x_{exp} - x_{WLC}(l, f_{exp})|) \quad (1)$$

The theoretical extension ($x_{WLC}(l_0,f_{exp})$) was determined using the elastic parameters (l_p, S) obtained from a WLC fit to the relaxation curve.

To determine the mechanical work ($W = F\Delta x$) performed to disrupt each KF–DNA contact in DNA stretching experiments, we determined the average rupture force and the extension of DNA released at every unpeeling event. This work is partially used to stretch the released DNA up to the rupture force. The rest of the work is dissipated into the solvent in the form of heat:

$$W_{dissipated} = \frac{F\Delta F}{k} - \Delta G_{stretching} \quad (2)$$

$$\Delta G_{stretching} = \frac{\Delta L}{L}\int_0^{x_{rup}} F_{WLC}(x)\, dx \quad (3)$$

where x_{rup} is the molecular extension of the DNA fiber at the rupture force. In the above expressions we use the fact that the force–extension curve of the WLC model is a sole function of x/L.

The model considered to reproduce the KF–DNA stretching curves simulates the contacts made between KF aggregates and DNA segments as a set of N noninteracting two-level systems. When force is applied to the molecule, each segment can yield an extension x_i in a thermally activated process characterized by a critical force f_c and a dissociation rate k_c. Each segment is described by its free energy of formation ΔG_i, activation barrier B_i, and distance to the transition state $x_i^{\ddagger}$. The released extension x_i was assumed to follow the experimental distribution (Figure 4b), and we introduced some structural disorder by assuming that ΔG and B are also exponentially distributed. Simulation parameters that best describe the experimental curves are $p(\Delta G) = (1/w)e^{-(\Delta G - \Delta G_0)/w}$ with $\Delta G \geq \Delta G_0$ = 10 k_BT and w = 1 k_BT; $x_i^{\ddagger}$ = 2 ± 1 nm; f_c = 5 ± 3 pN; k_c = 0.5 s^{-1}; $p(B) = (1/w')e^{-(B-B_0)/w'}$ with $B \geq B_0$ = 89 k_BT and w' = 5 k_BT. The contact-length distribution (x_i) was assumed to follow the experimental distribution $p(x_i) = (1/w)e^{-(x_i - x_{i,0})/w}$ for $x_i \geq x_{i,0}$ ($p(x_i)$ = 0 otherwise) with $x_{i,0}$ = 8 nm and w = 24 nm. Other specific parameters for the simulations shown in Figure 4d are k_{trap} = 0.07 pN/nm, v = 500 nm/s, l_p = 35 nm, and DNA slack = 6500 nm. Errors are an estimation of the range in which the features of the process are well reproduced by the model when each parameter is independently modified.

Sample Flow Setup. A syringe pump (PicoPump, KDScientific) and a glass syringe have been used for KF sample infusion. Polyethylene PE-10 tubing (BD Intramedic) is used to connect the syringe to the fluidics chamber. For the experiments performed with a constant force protocol a buffer flow-rate of 3 μL/min is used to keep a low drag force on the bead. For the other experiments a higher flow-rate of 9 μL/min was preferred (Supporting Information). The arrival of the KF solution into the experimental area can be monitored due to the slight change in the refractive index of the medium caused by the 2% DMSO content of the peptide buffer.

We were not able to establish DNA tethers between polystyrene beads with KF in the buffer, suggesting that strong condensation effects appear on untethered molecules. Therefore, experiments were always performed by flowing KF to DNA molecules that had been tethered in peptide-free buffer. Flow experiments performed with polystyrene beads without DNA do not show aggregation of KF onto the bead surfaces nor an increase in stickiness between beads, ruling out aggregation on bead surfaces.

AFM Sample Preparation and Imaging. KF–DNA reactions included 1.65 ng of DNA (0.9 nM dsDNA molecules, pGEM3Z, 2743 bp) (Promega) linearized with *Bam*HI and 100 μM KF in 20 mM Tris-HCl (pH 7.5) and 100 mM NaCl. To facilitate adsorption of DNA in a buffer devoid of Mg^{2+} ions, we pretreated the mica surface with 100 mM spermine tetrahydrochloride (S85610, Fluka, Sigma) dissolved in 10 mM Tris-HCl (pH 7.5). Pretreatment with spermine consisted in deposition of 20 μL of 100 mM spermine tetrahydrochloride on a freshly cleaved mica surface,

one-minute adsorption, washing with Milli-Q water, and drying with nitrogen gas. Use of spermine at low concentrations allowed uniform adsorption of DNA molecules. Immediately after the spermine treatment, the mixture of KF and DNA incubated at room temperature and for the stated time was deposited on the mica. After 30 s, the mica surface was washed with filtered-Milli-Q water and blown dry in a gentle stream of nitrogen gas. To study KF−ssDNA interactions, a stock of ssDNA was produced by heat denaturing the linearized pGEM plasmid at 95 °C for 5 min and placing the tube quickly after on ice. DNA molecules of ~3 kb remain stable in its ssDNA form following this procedure as long as they remain at 4 °C for at least one week. KF and ssDNA were mixed at the same proportions as for dsDNA and followed the sample preparation procedure described above. Samples were imaged in air at room temperature at identical conditions as previously described.[47] Standard image processing consisted of plane subtraction and flattening using WSxM freeware.[48]

Conflict of Interest: The authors declare no competing financial interest.

Acknowledgment. The authors thank Pharmamar SA and G. Acosta for providing the peptides kahalalide F and its analogue. J.C.S. acknowledges a grant associated with ICREA Academia 2008; F.R. is supported by the Human Frontier Science Program [Grant No. RGP55-2008], the Spanish Ministry of Economy and Competitiveness [Grant No. FIS2010-19342], and an ICREA Academia award; F.M.H. acknowledges a grant from the European Research Council [Starting Grant No. 206117] and the Spanish Ministry of Economy and Competitiveness [Grant No. FIS2011-24638]; M.E.F.P. was supported by a contract from CSIC [Contract No. 200920I123, associated with the ERC grant]. F.A. acknowledges CICYT [Grant No. CTQ2012-30930], and S.B.D. an invited professor position from AGAUR (Generalitat de Catalunya).

Supporting Information Available: Additional methods, optical tweezers results, DLS measurements, and AFM images. This material is available free of charge *via* the Internet at http://pubs.acs.org.

REFERENCES AND NOTES

1. Calamai, M.; Kumita, J.; Mifsud, J.; Parrini, C.; Ramazzotti, M.; Ramponi, G.; Taddei, N.; Chiti, F.; Dobson, C. Nature and Significance of the Interactions between Amyloid Fibrils and Biological Polyelectrolytes. *Biochemistry* **2006**, *45*, 12806–12815.
2. Bucciantini, M.; Giannoni, E.; Chiti, F.; Baroni, F.; Formigli, L.; Zurdo, J.; Taddei, N.; Ramponi, G.; Dobson, C.; Stefani, M. Inherent Toxicity of Aggregates Implies a Common Mechanism for Protein Misfolding Diseases. *Nature* **2002**, *416*, 507–511.
3. Gsponer, J.; Vendruscolo, M. Theoretical Approaches to Protein Aggregation. *Protein Pept. Lett.* **2006**, *13*, 287–293.
4. Coan, K.; Shoichet, B. Stoichiometry and Physical Chemistry of Promiscuous Aggregate-Based Inhibitors. *J. Am. Chem. Soc.* **2008**, *130*, 9606–9612.
5. Puchalla, J.; Krantz, K.; Austin, R.; Rye, H. Burst Analysis Spectroscopy: A Versatile Single-Particle Approach for Studying Distributions of Protein Aggregates and Fluorescent Assemblies. *Proc. Natl. Acad. Sci. U.S.A.* **2008**, *105*, 14400–14405.
6. Feng, B.; Toyama, B.; Wille, H.; Colby, D.; Collins, S.; May, B.; Prusiner, S.; Weissman, J.; Shoichet, B. Small-Molecule Aggregates Inhibit Amyloid Polymerization. *Nat. Chem. Biol.* **2008**, *4*, 197–199.
7. Coan, K.; Maltby, D.; Burlingame, A.; Shoichet, B. Promiscuous Aggregate-Based Inhibitors Promote Enzyme Unfolding. *J. Med. Chem.* **2009**, *52*, 2067–2075.
8. Braun, S.; Humphreys, C.; Fraser, E.; Brancale, A.; Bochtler, M.; Dale, T. Amyloid-Asssociated Nucleic Acid Hybridisation. *PLoS One* **2011**, *6*, e19125.
9. Di Domizio, J.; Zhang, R.; Stagg, L.; Gagea, M.; Zhuo, M.; Ladbury, J.; Cao, W. Binding with Nucleic Acids or Glycosaminoglycans Converts Soluble Protein Oligomers to Amyloid. *J. Biol. Chem.* **2012**, *287*, 736–747.
10. Macedo, B.; Millen, T.; Braga, C.; Gomes, M.; Ferreira, P.; Kraineva, J.; Winter, R.; Silva, J.; Cordeiro, Y. Nonspecific Prion Protein-Nucleic Acid Interactions Lead to Different Aggregates and Cytotoxic Species. *Biochemistry* **2012**, *51*, 5402–5413.
11. Motamedi-Shad, N.; Garfagnini, T.; Penco, A.; Relini, A.; Fogolari, F.; Corazza, A.; Esposito, G.; Bemporad, F.; Chiti, F. Rapid Oligomer Formation of Human Muscle Acylphosphatase Induced by Heparan Sulfate. *Nat. Struct. Mol. Biol.* **2012**, *19*, 547–554.
12. Cherny, D.; Hoyer, W.; Subramaniam, V.; Jovin, T. Double-Stranded DNA Stimulates the Fibrillation of α-Synuclein *in Vitro* and Is Associated with the Mature Fibrils: An Electron Microscopy Study. *J. Mol. Biol.* **2004**, *344*, 929–938.
13. Cohlberg, J.; Li, J.; Uversky, V.; Fink, A. Heparin and Other Glycosaminoglycans Stimulate the Formation of Amyloid Fibrils from α-Synuclein *in Vitro*. *Biochemistry* **2002**, *41*, 1502–1511.
14. Dale, T. Protein and Nucleic Acid Together: A Mechanism for the Emergence of Biological Selection. *J. Theor. Biol.* **2006**, *240*, 337–342.
15. Hamann, M. T.; Scheuer, P. J.; Kahalalide, F. A Bioactive Depsipeptide from the Sacoglossan Mollusk *Elysia rufescens* and the Green Alga *Bryopsis sp*. *J. Am. Chem. Soc.* **1993**, *115*, 5825–5826.
16. López-Macià, A.; Jiménez, J. C.; Royo, M.; Giralt, E.; Albericio, F. Synthesis and Structure Determination of Kahalalide F *J. Am. Chem. Soc.* **2001**, *123*, 11398–11401.
17. García-Rocha, M.; Bonay, P.; Avila, J. The Antitumoral Compound Kahalalide F Acts on Cell Lysosomes. *Cancer Lett.* **1996**, *99*, 43–50.
18. Suárez, Y.; González, L.; Cuadrado, A.; Berciano, M.; Lafarga, M.; Munoz, A.; Kahalalide, F. A New Marine-Derived Compound, Induces Oncosis in Human Prostate and Breast Cancer Cells. *Mol. Cancer Ther.* **2003**, *2*, 863–872.
19. Sewell, J. M.; Mayer, I.; Langdon, S. P.; Smyth, J. F.; Jodrell, D. I.; Guichard, S. M. The Mechanism of Action of Kahalalide F: Variable Cell Permeability in Human Hepatoma Cell Lines. *Eur. J. Cancer* **2005**, *41*, 1637–1644.
20. Molina-Guijarro, J.; Macías, Á.; García, C.; Muñoz, E.; García-Fernández, L.; David, M.; Núñez, L.; Martínez-Leal, J.; Moneo, V.; Cuevas, C.; *et al*. Irvalec Inserts into the Plasma Membrane Causing Rapid Loss of Integrity and Necrotic Cell Death in Tumor Cells. *PLoS One* **2011**, *6*, e19042.
21. Li, I.; Walker, G. Signature of Hydrophobic Hydration in a Single Polymer. *Proc. Natl. Acad. Sci. U.S.A.* **2011**, *108*, 16527–16532.
22. Huguet, J.; Forns, N.; Ritort, F. Statistical Properties of Metastable Intermediates in DNA Unzipping. *Phys. Rev. Lett.* **2009**, *103*, 248106.
23. Ritort, F.; Mihardja, S.; Smith, S. B.; Bustamante, C. Condensation Transition in DNA-Polyaminoamide Dendrimer Fibers Studied Using Optical Tweezers. *Phys. Rev. Lett.* **2006**, *96*, 118301.
24. Leger, J. F.; Romano, G.; Sarkar, A.; Robert, J.; Bourdieu, L.; Chatenay, D.; Marko, J. F. Structural Transitions of a Twisted and Stretched DNA Molecule. *Phys. Rev. Lett.* **1999**, *83*, 1066–1069.
25. Vladescu, I. D.; McCauley, M. J.; Nuñez, M. E.; Rouzina, I.; Williams, M. C. Quantifying Force-Dependent and Zero-Force DNA Intercalation by Single-Molecule Stretching. *Nat. Methods* **2007**, *4*, 517–522.
26. Huguet, J. M.; Bizarro, C. V.; Forns, N.; Smith, S. B.; Bustamante, C.; Ritort, F. Single-Molecule Derivation of Salt Dependent Base-Pair Free Energies in DNA. *Proc. Natl. Acad. Sci. U.S.A.* **2010**, *107*, 15431–15436.
27. Podgornik, R.; Jönsson, B. Stretching of Polyelectrolyte Chains by Oppositely Charged Aggregates. *Europhys. Lett.* **1993**, *24*, 501–506.
28. Brower-Toland, B.; Smith, C.; Yeh, R.; Lis, J.; Peterson, C.; Wang, M. Mechanical Disruption of Individual Nucleosomes Reveals a Reversible Multistage Release of DNA. *Proc. Natl. Acad. Sci. U.S.A.* **2002**, *99*, 1960–1965.
29. Skoko, D.; Yan, J.; Johnson, R.; Marko, J. Low-Force DNA Condensation and Discontinuous High-Force Decondensation Reveal a Loop-Stabilizing Function of the Protein Fis. *Phys. Rev. Lett.* **2005**, *95*, 208101.

30. Van Noort, J.; Verbrugge, S.; Goosen, N.; Dekker, C.; Dame, R. T. Dual Architectural Roles of HU: Formation of Flexible Hinges and Rigid Filaments. *Proc. Natl. Acad. Sci. U.S.A.* **2004**, *101*, 6969–6974.
31. Todd, B.; Rau, D. Interplay of Ion Binding and Attraction in DNA Condensed by Multivalent Cations. *Nucleic Acids Res.* **2008**, *36*, 501–510.
32. Hormeño, S.; Moreno-Herrero, F.; Ibarra, B.; Carrascosa, J. L.; Valpuesta, J. M.; Arias-Gonzalez, J. R. Condensation Prevails over B-A Transition in the Structure of DNA at Low Humidity. *Biophys. J.* **2011**, *100*, 2006–2015.
33. Yoshimura, Y.; Lin, Y.; Yagi, H.; Lee, Y.; Kitayama, H.; Sakurai, K.; So, M.; Ogi, H.; Naiki, H.; Goto, Y. Distinguishing Crystal-Like Amyloid Fibrils and Glass-Like Amorphous Aggregates from their Kinetics of Formation. *Proc. Natl. Acad. Sci. U.S.A.* **2012**, *109*, 14446–14451.
34. Ross, C.; Poirier, M. What is the Role of Protein Aggregation in Neurodegeneration? *Nat. Rev. Mol. Cell Biol.* **2005**, *6*, 891–898.
35. Ceci, P.; Cellai, S.; Falvo, E.; Rivetti, C.; Rossi, G.; Chiancone, E. DNA Condensation and Self-Aggregation of *Escherichia coli* Dps are Coupled Phenomena Related to the Properties of the N-Terminus. *Nucleic Acids Res.* **2004**, *32*, 5935–5944.
36. Ceci, P.; Mangiarotti, L.; Rivetti, C.; Chiancone, E. The Neutrophil-Activating Dps Protein of *Helicobacter pylori*, HP-NAP, Adopts a Mechanism Different from *Escherichia coli* Dps to Bind and Condense DNA. *Nucleic Acids Res.* **2007**, *35*, 2247–2256.
37. Hou, X.; Zhang, X.; Wei, K.; Ji, C.; Dou, S.; Wang, W.; Li, M.; Wang, P. Cisplatin Induces Loop Structures and Condensation of Single DNA Molecules. *Nucleic Acids Res.* **2009**, *37*, 1400–1410.
38. Dansithong, W.; Wolf, C.; Sarkar, P.; Paul, S.; Chiang, A.; Holt, I.; Morris, G.; Branco, D.; Sherwood, M.; Comai, L.; *et al*. Cytoplasmic CUG RNA *Foci* Are Insufficient to Elicit Key DM1 Features. *PLoS One* **2008**, *3*, e3968.
39. Dickson, A. M.; Wilusz, C. J. Repeat Expansion Diseases: When a Good RNA Turns Bad. *Wiley Interdiscip. Rev.: RNA* **2010**, *1*, 173–192.
40. García-López, A.; Llamus, B.; Orzáez, M.; Pérez-Payá, E.; Artero, R. *In Vivo* Discovery of a Peptide that Prevents CUG-RNA Hairpin Formation and Reverses RNA Toxicity in Myotonic Dystrophy Models. *Proc. Natl. Acad. Sci. U.S.A.* **2011**, *108*, 11866–11871.
41. Smith, S. B.; Cui, Y.; Bustamante, C. Optical-Trap Force Transducer that Operates by Direct Measurement of Light Momentum. *Methods Enzymol.* **2002**, *361*, 134–162.
42. Smith, S.; Cui, Y.; Bustamante, C. Overstretching B-DNA: the Elastic Response of Individual Double-Stranded and Single-Stranded DNA Molecules. *Science* **1996**, *271*, 795–799.
43. Wang, M. D.; Yin, H.; Landick, R.; Gelles, J.; Block, S. M. Stretching DNA with Optical Tweezers. *Biophys. J.* **1997**, *72*, 1335–1346.
44. Baumann, C. G.; Smith, S. B.; Bloomfield, V. A.; Bustamante, C. Ionic Effects on the Elasticity of Single DNA Molecules. *Proc. Natl. Acad. Sci. U.S.A.* **1997**, *94*, 6185–6190.
45. Bouchiat, C.; Wang, M.; Allemand, J.; Strick, T.; Block, S.; Croquette, V. Estimating the Persistence Length of a Worm-Like Chain Molecule from Force-Extension Measurements. *Biophys. J.* **1999**, *76*, 409–413.
46. Marquardt, D. W. An Algorithm for Least-Squares Estimation of Nonlinear Parameters. *J. Soc. Ind. Appl. Math.* **1963**, *11*, 431–441.
47. Fuentes-Perez, M. E.; Gwynn, E. J.; Dillingham, M. S.; Moreno-Herrero, F. Using DNA as a Fiducial Marker to Study SMC Complex Interactions with the Atomic Force Microscope. *Biophys. J.* **2012**, *102*, 839–848.
48. Horcas, I.; Fernández, R.; Gómez-Rodrguez, J. M.; Colchero, J.; Gómez-Herrero, J.; Baro, A. M. WSXM: A Software for Scanning Probe Microscopy and a Tool for Nanotechnology. *Rev. Sci. Instrum.* **2007**, *78*, 013705–013705.